Available online at www.sciencedirect.com

jmr&t Journal of Materials Research and Technology

journal homepage: www.elsevier.com/locate/jmrt

Original Article

Microstructure evolution of graphene reinforced Cu/CeO_2/Cr electrical contact materials under thermal deformation behavior

Lihua Li [a,b,c,**,1], Shuang Liu [a,b,c,1], Meng Zhou [a,b,c,1,***], Yi Zhang [a,b,c,*], Shengli Liang [a,b,c], Jinliang Huang [a,b,c,****], Baohong Tian [a,b,c], Yongfeng Geng [a,d], Yijie Ban [a,e], Yong Liu [a,b,c], Yanlin Jia [f], Xu Li [g], Alex A. Volinsky [h]

[a] School of Materials Science and Engineering, Henan University of Science and Technology, Luoyang, 471023, China
[b] Provincial and Ministerial Co-construction of Collaborative Innovation Center for Non-ferrous Metal New Materials and Advanced Processing Technology, Henan Province, Luoyang, 471023, China
[c] Henan Province Key Laboratory of Nonferrous Materials Science and Processing Technology, Luoyang, 471023, China
[d] State Key Laboratory of Metal Matrix Composites, Shanghai Jiao Tong University, Shanghai 200240, China
[e] College of Materials Science and Engineering, Huazhong University of Science and Technology, Wuhan, 430074, China
[f] School of Materials Science and Engineering, Central South University, Changsha, 410083, China
[g] Center for Advanced Measurement Science, National Institute of Metrology, Beijing, 100029, China
[h] Department of Mechanical Engineering, University of South Florida, Tampa, 33620, USA

ARTICLE INFO

Article history:
Received 6 January 2022
Accepted 6 March 2022
Available online 11 March 2022

Keywords:
Graphene
Hot deformation
Flow stress

ABSTRACT

The effect of graphene on the thermal deformation of Cu/CeO_2/Cr and GO-Cu/CeO_2/Cr composites was studied. The isothermal compression test was carried out with Gleeble-1500D thermomechanical simulation device in the range of 600–900 °C and strain rate of 0.001–1 s^{-1}. The microstructure after deformation was characterized and analyzed by optical microscope, scanning electron microscope (SEM), transmission electron microscope (TEM) and electron backscatter diffraction (EBSD). The interaction of work hardening, dynamic recovery and dynamic recrystallization was described. The constitutive equation was successfully established. The results show that Cr particles are extruded into strips, and nano CeO_2 particles nail dislocations, which inhibit dynamic recovery and dynamic

* Corresponding author. School of Materials Science and Engineering, Henan University of Science and Technology, Luoyang, 471023, China.
** Corresponding author. School of Materials Science and Engineering, Henan University of Science and Technology, Luoyang, 471023, China.
*** Corresponding author. School of Materials Science and Engineering, Henan University of Science and Technology, Luoyang, 471023, China.
**** Corresponding author. School of Materials Science and Engineering, Henan University of Science and Technology, Luoyang, 471023, China.
E-mail addresses: lilihua7818@163.com (L. Li), zhoumeng0902@126.com (M. Zhou), yizhang@huast.edu.cn (Y. Zhang), huangjl@haust.edu.cn (J. Huang).
[1] These authors contributed equally to this work.
https://doi.org/10.1016/j.jmrt.2022.03.038

Electron backscattered diffraction (EBSD)
Constitutive equations

recrystallization. Dispersion strengthening, twin strengthening and grain refinement strengthening occur the thermal deformation of GO-Cu/CeO_2/Cr composites, increase the flow stress and activation energy of the composites, and inhibit the dynamic recrystallization of the composites. When the hot deformation temperature increases, the texture orientation is strengthened. GO-Cu/CeO_2/Cr composites have typical dynamic recovery characteristics and high temperature properties.

1. Introduction

Nowadays, electronic control systems are widely used in both electronic and electrical engineering and national defense technology. One of the results of this automation process is the wide use of sensors and electrical connectors, which indirectly promotes the sustainable use of electrical contacts and tests their ability to transmit information [1,2]. Electrical contact materials are widely used in vacuum switches and high voltage circuits. The performance of electrical contact materials is one of the key factors affecting the working characteristics of switchgear and the service life of electrical appliances. However, the pure metal contact material with high melting point has many disadvantages, such as breaking current and high level of current cut-off, which limits its application range [3]. With the development in recent years, nano particle reinforced metal matrix composites have gradually become an important part of national defense, rail transit, aerospace, electronics industry and so on. With a series of excellent properties such as high conductivity, excellent thermal conductivity and excellent corrosion resistance, copper is used as contact wire, lead frame and electrical contact material of high-speed railway, and then widely used in electrical and electronic, household appliances, aerospace, and other fields [4–8]. Graphene copper matrix composites have the advantages of high conductivity, thermal conductivity, good plasticity of copper matrix and high strength and super toughness of graphene. The addition of Cr in GO-Cu/CeO_2/Cr composites can significantly improve the hardness and wear resistance of the composites. The addition of CeO_2 nanoparticles can fix dislocations, produce dislocation entanglement, and improve the strength of materials.

With the development of computer science and numerical simulation technology, the research on the thermal deformation behavior of materials is becoming more and more extensive. The thermal deformation of materials is the basis of thermal processing and can be used to improve the properties of materials [9], which is widely used in handicraft manufacturing. The process of material thermal deformation is also a process of thermal activation, and its deformation behavior can be described by the relationship between deformation temperature, deformation rate and flow stress. Yang et al. [10] studied the effect of rare earth Y on the microstructure evolution of Cu-Co-Si alloy during hot deformation. The results show that the addition of 0.2 wt% Y can promote the nucleation of dynamic recrystallization (DRX) grains and the growth of DRX grains, and rare earth nanoparticles can interact with dislocations to improve the deformation resistance during thermal deformation. Hiraoka [11] et al. conducted compression experiments on W-80vol%Cu composites at room temperature. It is found that with the increase of strain rate, fibrous structure gradually appears in the grains of the composites. Zhang et al. [12,13] prepared Al_2O_3-Cu/(W, Cr) composites by vacuum hot pressing sintering and internal oxidation. The effects of nano-Al_2O_3 and W particles on the thermal deformation of Al_2O_3-Cu/(W, Cr) composites at different temperatures and strain rates were studied. It is found that the flow stress increased with the increased of strain rate and decreased with the increased of deformation temperature. Ban and others [14] found that the flow stress decreased with the increased of deformation temperature and the decreased of deformation rate after thermal deformation of Cu-Ni-Co-Si and Cu-Ni-Co-Si-Cr alloys in the range of 500–900 °C. The addition of Cr can refine the grains and improve the activation energy of materials.

Previous studies mainly focused on the aging precipitation behavior of alloys during hot deformation, while few studies on the hot deformation behavior of composites. In this work, the thermal deformation behavior of Cu/CeO_2/Cr and GO-Cu/CeO_2/Cr composites was studied by isothermal compression test on Geeble-1500D thermomechanical simulator. The microstructure evolution and flow stress behavior at deformation temperature of 600–900 °C and strain rate of 0.001–1 s^{-1} were studied. The microstructure and orientation of the composites under different process conditions were analyzed, and the constitutive equations of Cu/CeO_2/Cr and GO-Cu/CeO_2/Cr composites were established.

2. Experiment materials and procedures

The average particle size of copper powder is 5–10 μm. The purity is 99.95%, which is provided by Nangong Xiangfan alloy material Co., Ltd. The average particle size of chromium powder is 44 μm and the purity is 99.95%, which is provided by Beijing Xingrongyuan Technology Co., Ltd. Ceria powder, with an average particle size of 50 nm (purity of 99.95%), is provided by Shanghai Aladdin Biochemical Technology Co., Ltd. Graphite powder (purity≥99.5%, 300 mesh), concentrated sulfuric acid (drug content 95%–98%), sodium nitrate (content≥99%), potassium permanganate (content ≥99.5%) shall be weighed in the proportion of 1 g: 30 ml: 0.5 g: 6 g. A certain

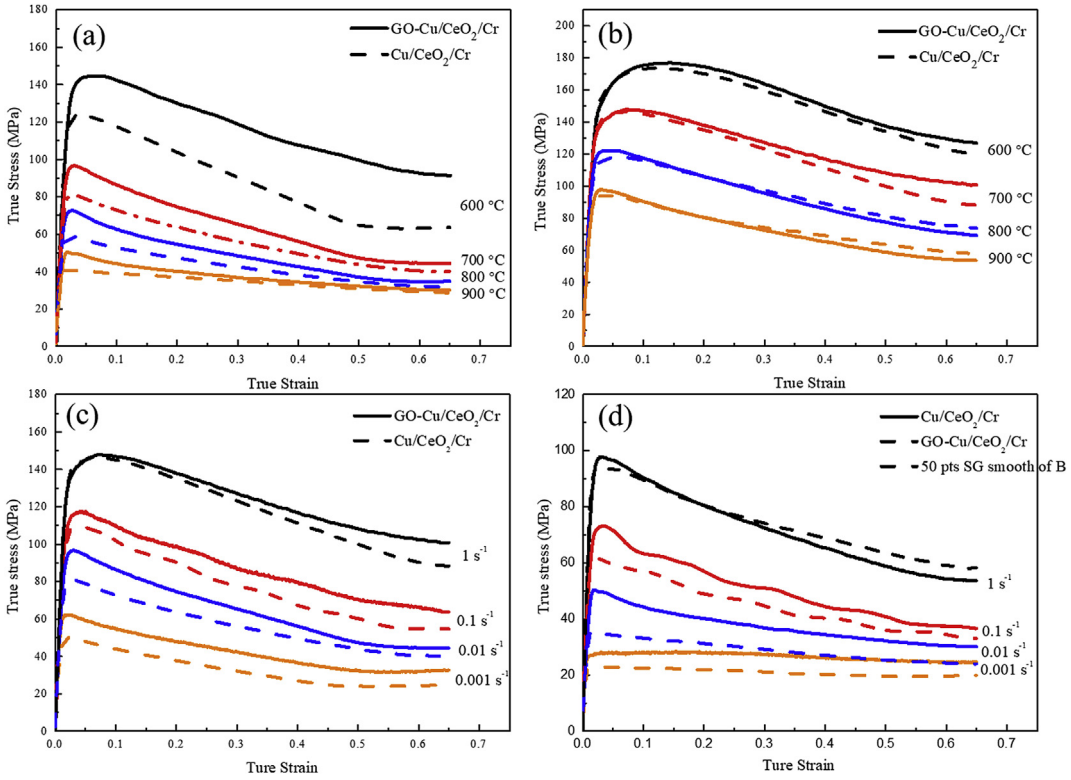

Fig. 1 – True stress-true strain curves of GO-Cu/CeO_2/Cr composite at different temperatures and strain rates: (a) 0.01 s^{-1};(b) 1 s^{-1};(c) 700 °C; (d) 900 °C.

amount of GO and cerium oxide prepared by the improved Hummers' method were dissolved in deionized water, and the suspension was prepared by ultrasonic dispersion (KQ-100 ultrasonic cleaning agent). The milled copper chromium composite powder (QM-3SP2 planetary mill) is added, mechanically stirred (JJ-1) for 30 min, and the composite powder is obtained after freeze-drying, the addition amount of CeO_2 is 0.5 wt.%, the addition amount of GO is 0 and 0.5 wt.%. Graphene and nano particle reinforced Cu-Cr electrical contact materials were prepared by densification method in spark plasma sintering furnace (SPS-20T-10). Process parameters of spark plasma sintering: the heating rate is 100 °C/min, when the temperature rises to 600 °C, the pressure is 30 MPa, the sintering temperature is 900 °C, the heat preservation is 10 min, and it is cooled with the furnace. The sintered composite was cut to size Φ8 × 12 mm cylindrical specimen. Isothermal axial thermal compression test was carried out on Gleeble-1500D thermal simulation test machine. When the deformation temperature is set at 600 °C, 700 °C, 800 °C and 900 °C, the strain rate is 0.001 s^{-1}, 0.01 s^{-1}, 0.1 s^{-1} and 1 s^{-1} respectively, and the heating rate is 10 °C/min. In order to make the sample temperature uniform, the sample was stored, preheated for 3–5 min in advance, and then isothermal axial compression was started. After deformation, quickly take out the sample and quench with water to maintain the high-temperature structure. The cutting direction of the sample is parallel to the deformation direction. After the sample is cut into thin sheets, the central part is used for polishing. The sample was etched in 5g $FeCl_3$, 10 ml HCl and 100 ml distilled water solution. The metallographic structure was observed by OLYMPUS PMG3 metallurgical microscope. After ion thinning, the EBSD image was observed by JMS-7800F field emission scanning electron microscope. The scanning step was 0.1 μm and the voltage was 20 kV. Software Transmission Channel 5 was used to analyze EBSD data. TEM and HRTEM images were obtained at 200 kV voltage and 0.19 nm resolution using JEM-2100F transmission electron microscope [15,16].

3. Results

3.1. *True stress-true strain curves*

The true stress-true strain curves of GO-Cu/CeO_2/Cr composite at 0.01 s^{-1}, 1 s^{-1}, 700 °C, 900 °C is shown in Fig. 1. Under the same thermal compression conditions, the addition of GO improves the stress of the composite. On the one hand, the addition of CeO_2 refines the grains of the alloy and improves the strength of the alloy, CeO_2 nanoparticles nail grain boundaries and dislocations, and finally improve the stress of the composites. The plastic deformation mechanism is revealed according to the different variation trends of the curve. Generally speaking, the hot deformation process of alloys has three typical characteristics: work hardening, dynamic recovery, and dynamic recrystallization [17]. At the initial stage of strain, with the increase of strain, the reinforced phase particles in the composite hinder the dislocation movement. The difficulty of dislocation movement leads to dislocation entanglement and dislocation accumulation and overlap. The dislocations in the composite

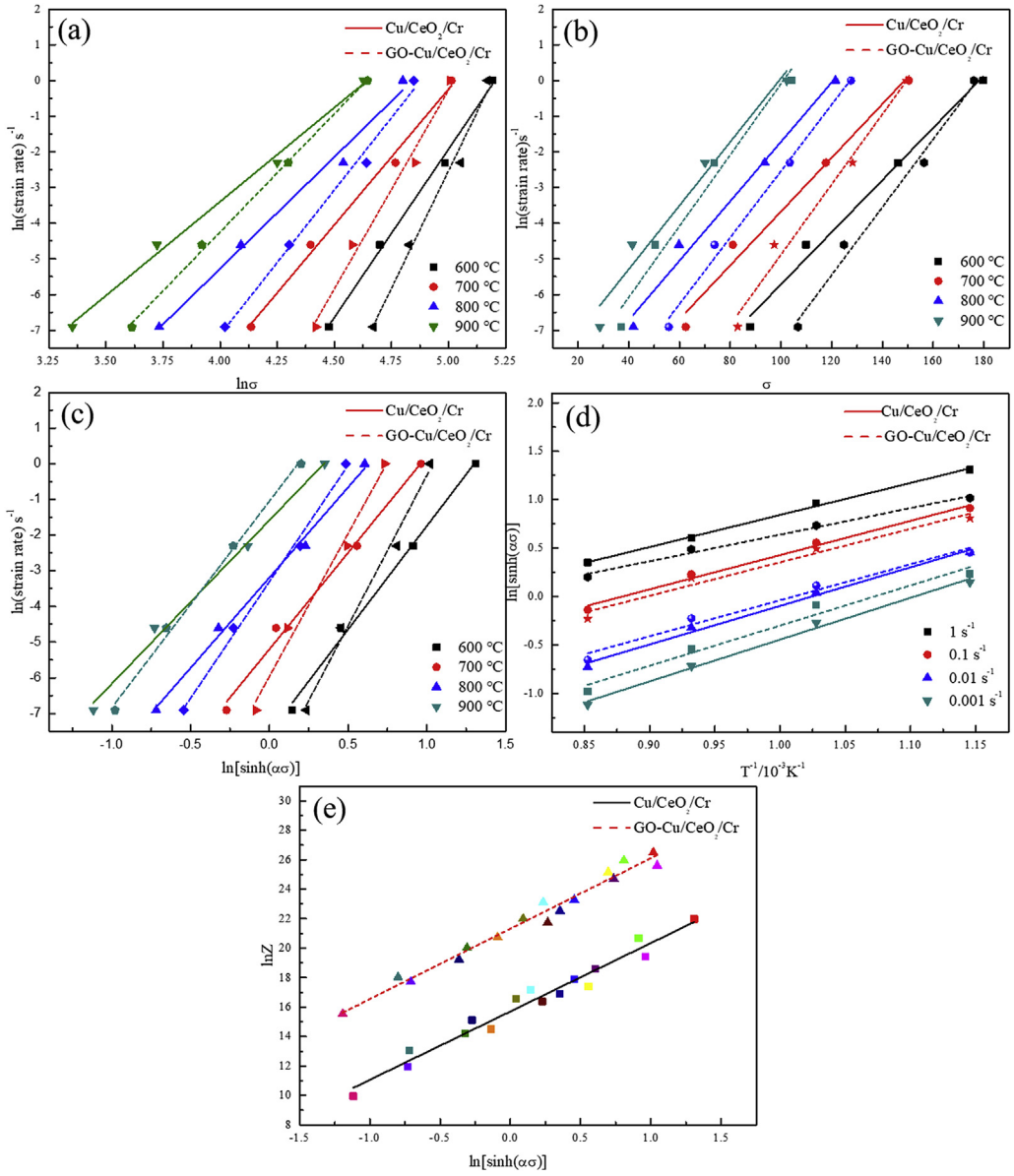

Fig. 2 – Relationship between:(a) ln ε̇-ln σ; (b) ln ε̇-σ; (c) ln ε̇-ln [sinh (ασ)]; (d) ln [sinh (ασ)]-$T^{-1} \times 10^3$ K^{-1}; (e) ln Z-ln [sinh (ασ)] of the Cu/CeO_2/Cr and GO-Cu/CeO_2/Cr composite.

proliferate rapidly, and the dislocation entanglement increases the dislocation resistance and produces obvious work hardening [18], during the work hardening stage, the slip surface and the lattice are distorted, and dislocations are entangled with strong interactions. At this time, the strength of the material increases significantly, but the further processing of the material can be hindered due to the decrease of plasticity. The true stress of composite material increases rapidly when the strain is small, after entering the steady-state stage, the dislocation density in this stage is large. At high temperature, the dislocation begins to rearrange the irregular dislocations through climbing and sliding, and the dynamic recovery and dynamic recrystallization also begin to occur in this stage. Therefore, the rheological softening effect occurs, and most of the processing hardening is offset to reach the steady-state rheological stage. Therefore, the flow stress gradually decreases and tends to be stable, or the flow stress continues to decrease until the end of thermal deformation [19–21]. In the process of dynamic recovery, the cross slip of dislocations plays an important role, including the decrease of defect density, the neutralization of reverse dislocations and the increase of defects. In addition, the magnitude of flow stress is mainly affected by strain rate and deformation temperature [22–24]. The flow stress decreases with the increase of temperature or the decrease of strain rate. For example, when the strain rate is 1 s^{-1} and the temperature increases from 600 °C to 900 °C, the peak stress of GO-Cu/CeO_2/Cr composites decreases from 174 MPa to 98 MPa. The average kinetic energy of atoms increases with the increase of temperature, which reduces the critical slip shear force of the composites and makes the dislocation movement and thermal diffusion more active. Therefore, the increase of deformation temperature promotes the nucleation and growth of

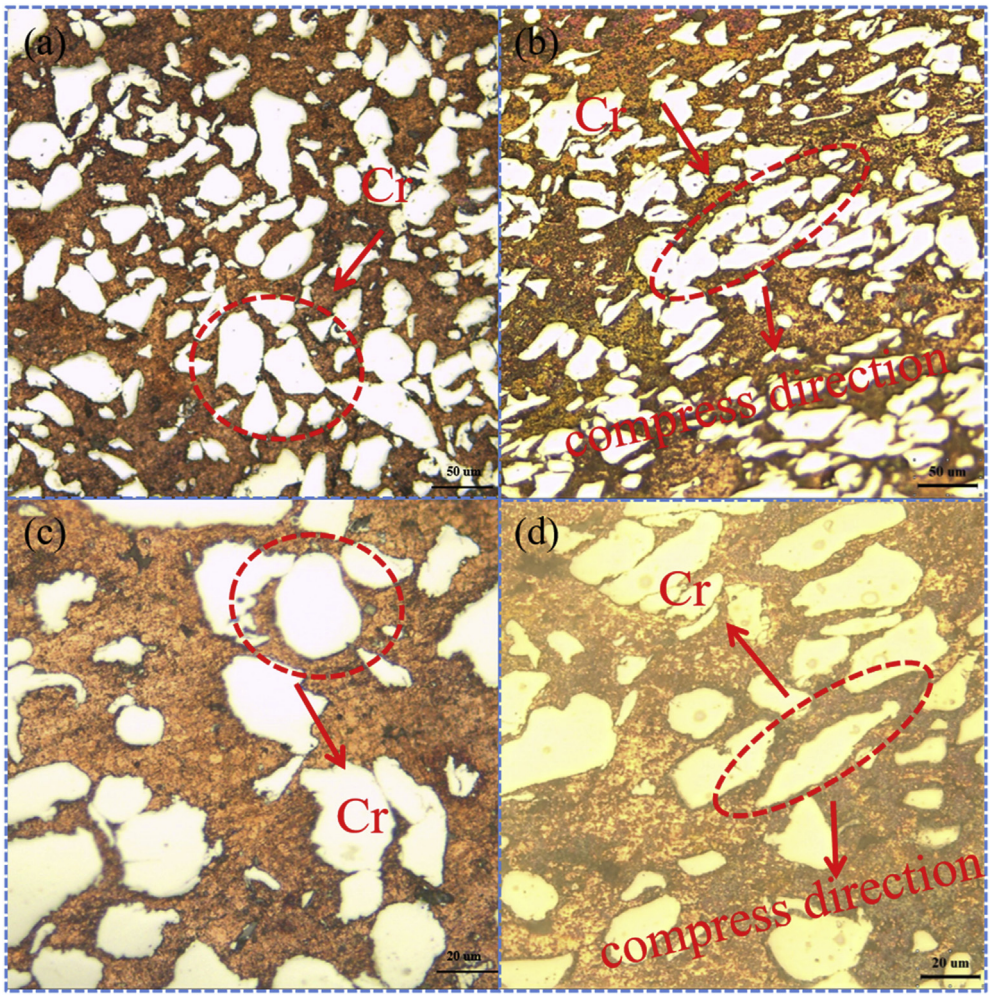

Fig. 3 – Optical microscope images of two composites under different conditions:(a) Sintered Cu/CeO_2/Cr composite; (b) Cu/CeO_2/Cr composite at 900 °C and 0.1 s^{-1} deformation; (c) Sintered GO-Cu/CeO_2/Cr composite; (d) GO-Cu/CeO_2/Cr composite under 900 °C 0.1 s^{-1} deformation.

dynamically recrystallized grains [25]. When the deformation temperature is 700 °C, the peak stress of GO-Cu/CeO_2/Cr composites decreases from 148 MPa to 62 MPa with the strain rate decreasing from 1 to 0.001 s^{-1}. The reason is that low strain rate provides sufficient time for dynamic recrystallization, and the dislocation increment is relatively flat at low strain rate, so the stress of composites is low at low strain rate. The most typical characteristic in the process of thermal deformation is the change of flow stress. In conclusion, under the condition of low strain rate (0.001 s^{-1}, 0.01 s^{-1}), the true stress-true strain curves show obvious dynamic recrystallization characteristics. Under the high strain rate (0.1 s^{-1}, 1 s^{-1}), when the composite deforms at low temperature of 600 °C, work hardening is dominant and the flow stress increases continuously. At 900 °C, dynamic recrystallization mainly controls the thermal deformation process. Therefore, small strain rate and high temperature are conducive to the dynamic softening process [26].

3.2. *Constitutive equation*

In order to further understand the thermal deformation behavior and deformation mechanism of graphene and nano CeO_2 reinforced copper matrix composites, the deformation temperature (T/°C) and strain rate ($\dot{\varepsilon}/s^{-1}$) effect on flow stress (σ/MPa) can provide a theoretical basis for the hot working of copper alloy. Sellars C M [27] described the constitutive Eq. (1) of thermal deformation behavior under all stress levels through experiments:

$$\dot{\varepsilon} = A_1\sigma^{n_1}\exp\left[-\frac{Q}{RT}\right] \quad \alpha\sigma < 0.8 \tag{1}$$

$$\dot{\varepsilon} = A_2\exp(\beta\sigma)\exp\left[-\frac{Q}{RT}\right] \quad \alpha\sigma < 1.2 \tag{2}$$

$$\dot{\varepsilon} = A[\sinh(\alpha\sigma)]^n\exp\left[-\frac{Q}{RT}\right] \quad (for\ all) \tag{3}$$

Zener [28] proposed to use temperature and deformation rate to express the influence on self-diffusion activation energy Z during thermal deformation:

$$Z = \dot{\varepsilon}\exp\left[\frac{Q}{RT}\right] = [\sinh(\alpha\sigma)]^n \tag{4}$$

Take logarithm on both sides of the equation:

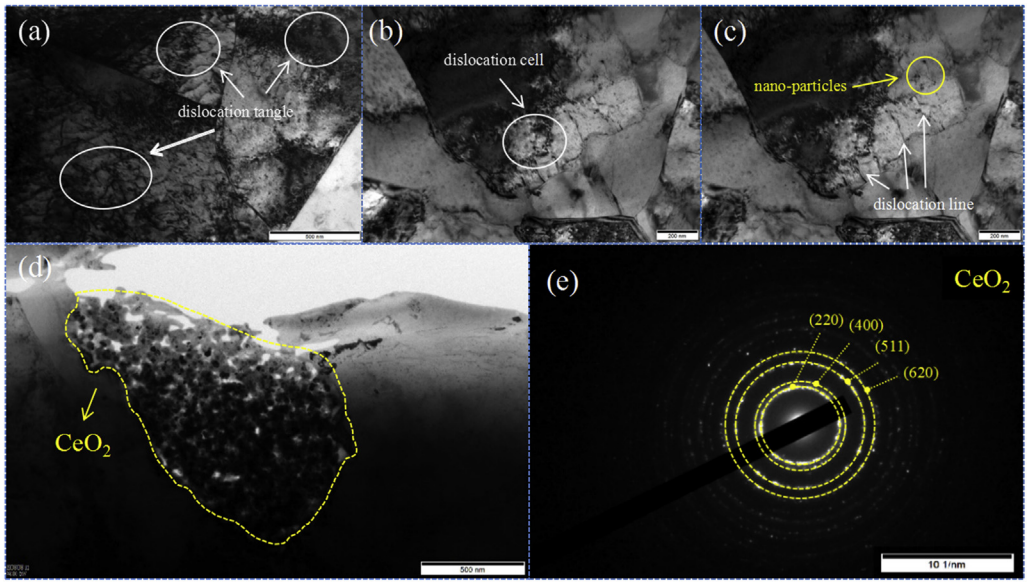

Fig. 4 – Microstructure of GO-Cu/CeO_2/Cr composite: (a) Dislocation entanglement, (b) Dislocation cell, (c) Dislocation lines and nanoparticles, (d) CeO_2 particles, (e) SADP of the CeO_2 particles in (d).

$$\ln\dot{\varepsilon} = n_1 \ln\sigma + \ln A_1 - \frac{Q}{RT} \tag{5}$$

$$\ln\dot{\varepsilon} = \beta\sigma + \ln A_2 - \frac{Q}{RT} \tag{6}$$

$$\ln Z = \ln A + n\ln[\sinh(\alpha\sigma)] \tag{7}$$

Take partial derivatives on both sides of Eq. (3) to obtain the thermal deformation activation energy:

$$Q = R\left[\frac{\partial(\ln\dot{\varepsilon})}{\partial\ln[\sin\alpha\sigma]}\right]_T \left[\frac{\partial\ln[\sinh\alpha\sigma]}{\partial(1/T)}\right] = RnS \tag{8}$$

In the above formula, Q is the thermal activation energy (J/mol), R is the general gas constant (8.314 J/mol·K), A,A_1,A_2,-n,n_1,α,β are constants. Where n_1 and β is the average value of the slope in Fig. 2 (a) and Fig. 2 (b), expressed as ln respectively lnε̇-lnσ and lnε̇-σ, the relationship between b and S is the average of the slopes in Fig. 2 (c) and Fig. 2 (d), respectively. Fig. 2 (e) shows the linear relationship between ln Z and ln [sinh (ασ)]. Where ln A is the intercept of Fig. 2 (e). Take GO-Cu/CeO_2/Cr composite as an example, n_1 = 9.7596, β = 0.0966, α = β/n_1 = 0.0099, n = 7.1862, S = 3.51704, ln A = 21.31989, A = $e^{21.31989}$. Thermal deformation activation energy:

$$Q = RnS = 8.314 \times 7.1862 \times 3.51704 = 210.130\ KJ/mol$$

Therefore, the constitutive equation of Cu/CeO_2/Cr composite is:

$$\dot{\varepsilon} = e^{15.70255}[\sinh(0.0112\sigma)]^{5.2143}\exp\left[-\frac{164174}{8.314T}\right] \tag{9}$$

The constitutive equation of GO-Cu/CeO_2/Cr composite is:

$$\dot{\varepsilon} = e^{21.31989}[\sinh(0.0099\sigma)]^{7.1862}\exp\left[-\frac{210130}{8.314T}\right] \tag{10}$$

Compared with Cu/CeO_2/Cr, the thermal deformation activation energy of the GO-Cu/CeO_2/Cr composite increased by 27.99%, which indicates that the addition of GO can enhance the high temperature stability of the composite. The reason may be that there is a large difference in thermal expansion coefficient between graphene and matrix. During thermal deformation, the movement of dislocation at the interface between graphene and matrix is hindered, forming dislocation climbing [29]. In addition, the addition of graphene hinders the diffusion of copper atoms and leads to the grain refinement of the composite, to achieve the effect of fine grain strengthening, and these are the reasons why activation energy can be increased [30].

3.3. *Microstructure analysis*

Fig. 3 is an optical microscope image of two composites after thermal compression under the same conditions. It can be seen from Fig. 3. (a) and (c) that the microstructure of the sintered sample is dense without obvious defects such as holes. Cr particles are evenly distributed on the copper matrix without obvious agglomeration. Fig. 3 (b) and (d) show the microstructure of two samples after deformation at 900 °C. As can be seen from figures, after hot extrusion deformation, the grain becomes thinner and narrower, the Cr particles are extruded into strips, and the strips are elongated along the vertical compression direction.

The microstructure evolution of the material after deformation is further explained by TEM characterization, as shown in Fig. 4. Due to work hardening, deformed grains and slip dislocations are generated at stress concentrations such as grain boundaries, as shown in Fig. 4 (a) and (b). The matrix on both sides of the sub grain boundary has a large number of dislocation entanglements and dislocation cellular substructures, in which the high-density entangled dislocations are mainly concentrated around the cell wall

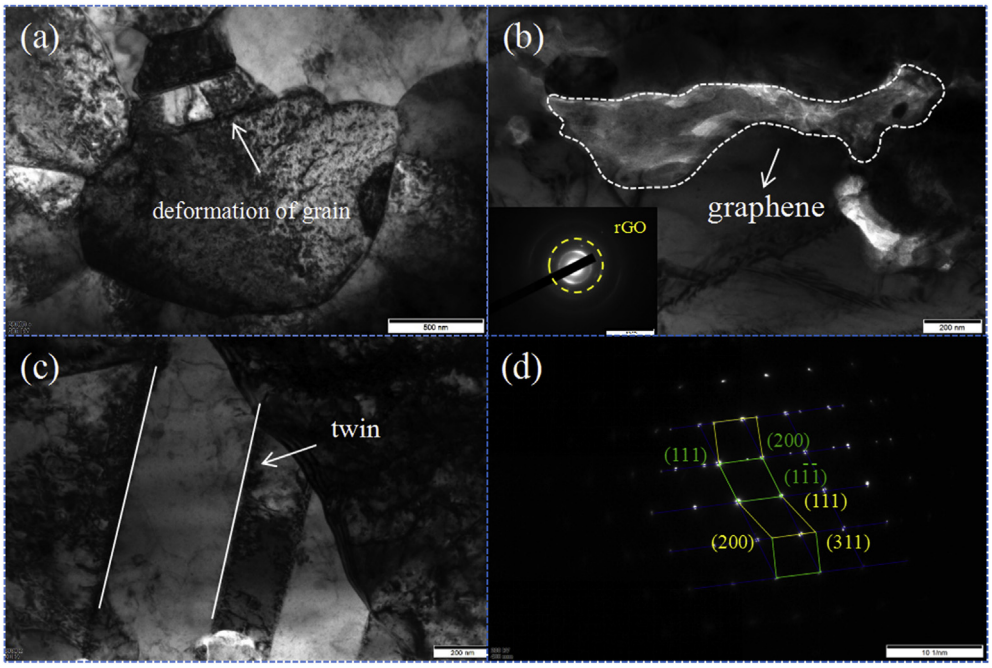

Fig. 5 – Microstructure of GO-Cu/CeO_2/Cr composite: (a) Deformed grain, (b) Graphene, (c) Twins, (d) Diffraction spots of twins.

(high-density dislocation cell wall). Due to the existence of grain boundary and a large number of dislocations are fixed by nanoparticles, the dislocation entanglement occurs, and there are many dislocation lines in the tissue due to deformation, at the same time, there are many nanoparticles around the dislocation line. The interaction between nanoparticles and dislocation line will improve the stress-strain curve of the composite in Fig. 4 (c) and (d). According to the selected area electron diffraction pattern, the particles are nano CeO_2 particles in Fig. 4 (e). The smaller ceria nanoparticles optimize the interface between graphene and metal matrix and reduce the probability of interface defects during thermal deformation. In addition, when dislocation entanglement leads to slip, nanoparticles fix dislocations,

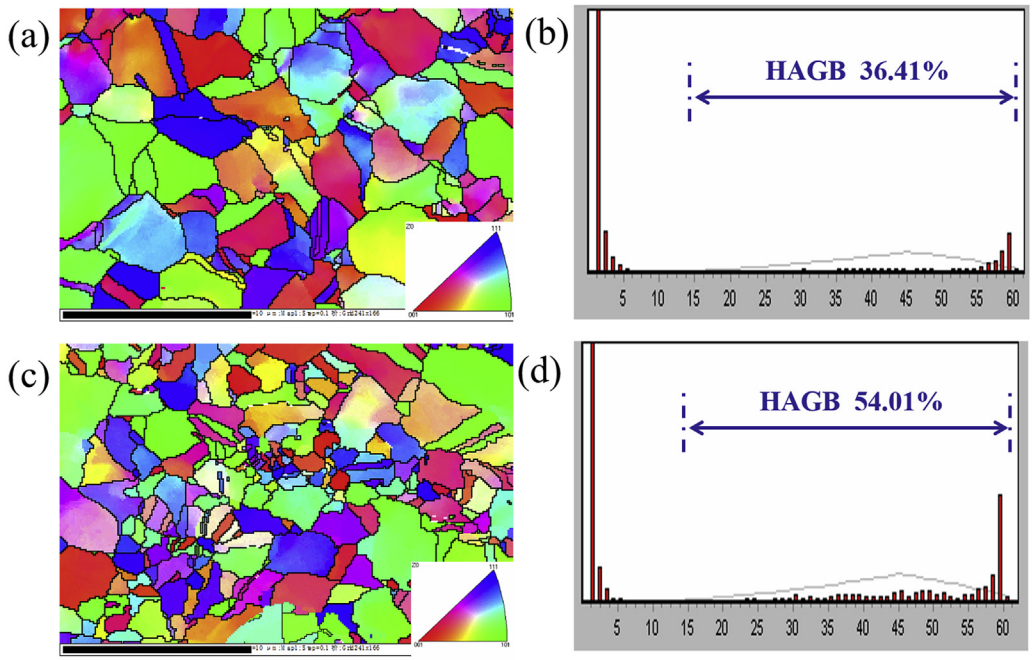

Fig. 6 – EBSD orientation diagram and misorientation angle distribution of. GO-Cu/CeO_2/Cr composites under different thermal deformation conditions: (a, b) 700 °C, 0.01 s^{-1}; (c, d) 900 °C , 0.01 s^{-1}.

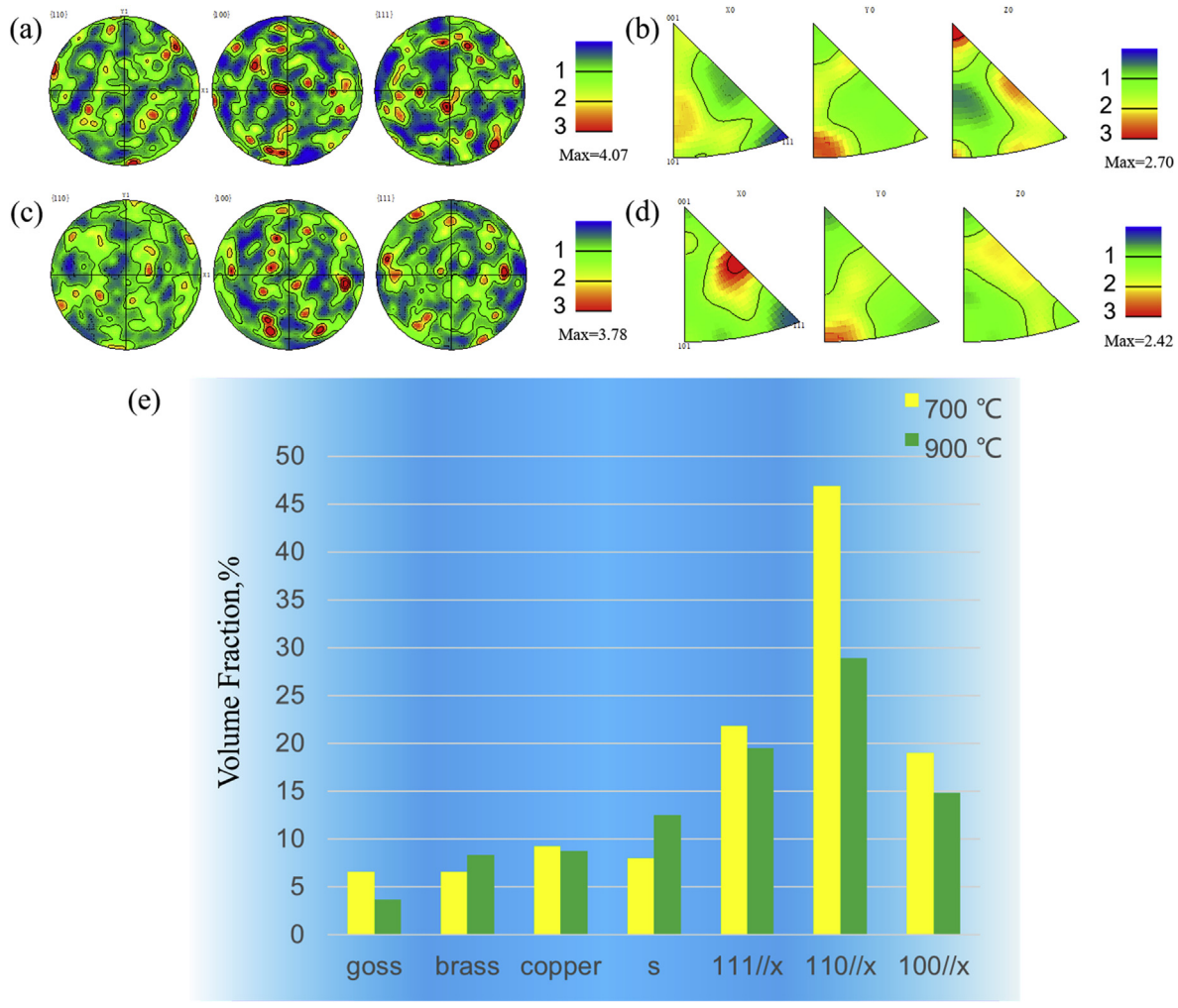

Fig. 7 – Pole figures, inverse pole figures of GO-Cu/CeO_2/Cr composites under different thermal deformation conditions: (a, b) 700 °C, 0.01 s^{-1}; (c, d) 900 °C, 0.01 s^{-1}; (e) Volume fraction of texture of different components.

further promote the crystal slip and deformation process, nail the grain boundary migration, and improve the material strength [31].

In the process of thermal deformation, in order to achieve the same deformation during compression, the deformation degree of coarse grains is greater than that of fine grains. The deformation of fine grains mainly occurs at the grain boundary, while the deformation of coarse grains occurs not only at the grain boundary, but also inside the grains, as shown in Fig. 5 (a). The diffraction spots of flake graphene are calibrated, and the results are shown in Fig. 5 (b). Twins formed in copper matrix hinder dislocation movement and grain boundary migration. In recent years, the introduction of twins into copper has been proved to be an effective method to improve strength and ductility. Like the traditional grain boundary, the twin boundary is a special coherent grain boundary, which hinders the movement of dislocations [32], and plays an important role in the strengthening of materials. The twins formed in the copper matrix hinder the dislocation movement and grain boundary migration, and play an important role in the strengthening of the material. It should be noted that the dislocation density around the twins is high, while the dislocation density inside the twins is low. This may be because the formation of twins consumes the dislocations and leads to the decrease of dislocation density [33]. The twin diffraction spots are calibrated, and the results are shown in Fig. 5 (c) and (d)

3.4. *EBSD analysis*

EBSD can be used to analyze the microstructure and orientation of solid crystal materials under different processing conditions [34,35]. In addition, the textures of face-centered cubic metals include the {011} <100> Goss texture, {112} <111> copper texture, {111} <211>R texture, {001} <100> cubic texture and {011} <211> brass texture [36,37]. Cu is a face-centered cubic crystal<001>, <101>, <111> orientation forms a triangle to indicate orientation in a crystal [38]. In order to study the texture and orientation angle of Cu/CeO_2/Cr and GO-Cu/CeO_2/Cr composites during thermal deformation, the samples were observed by JSM-7800F backscattering scanning electron microscope. Fig. 6 shows EBSD orientation of GO-Cu/CeO_2/Cr composite under isothermal compression at 700 °C, 0.01 s^{-1} and 900 °C, 0.01 s^{-1}. There are three main colors in the orientation diagram, mainly due to the different orientation of the grains. As shown in Fig. 6 (a) and (c), after isothermal compression test, the grain deformation is serious. As the

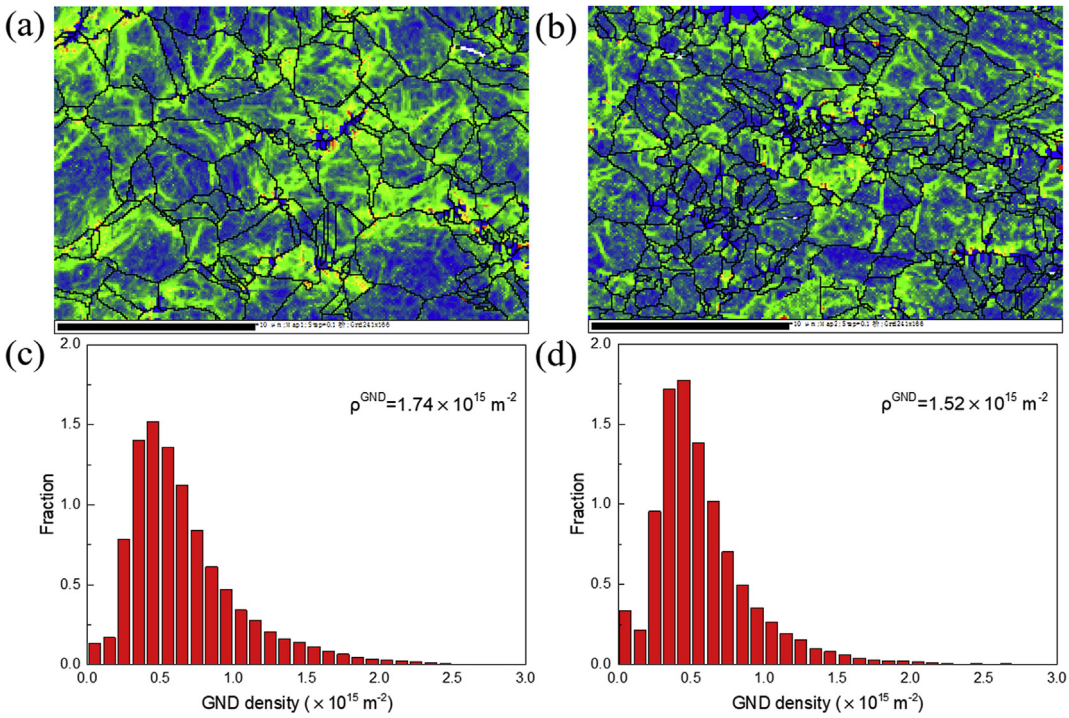

Fig. 8 – EBSD-IPF and corresponding KAM maps of GO-Cu/CeO_2/Cr composites under different thermal deformation conditions: (a, c, e) 700 °C, 0.01 s^{-1}; (b, d, f) 900 °C, 0.01 s^{-1}.

deformation temperature increases to 900 °C, the fine recrystallized grains gradually disappear, and the deformed grains are replaced by the growing recrystallized grains. Therefore, the increase of temperature provides power for the dynamic recrystallization of grains and promotes the occurrence of dynamic recrystallization. As can be seen from Fig. 6 (b) and (d), the distribution law of orientation angle is roughly the same, and it is quite concentrated at low dislocation angle, which is related to storage dislocation [39], and the concentration of low error angle and high error angle is almost the same. When the deformation temperature is low, a large number of deformed grains and low angle grain boundaries appear (LAGBs, misorientation angle<15°), with the increase of deformation temperature, the content of high angle grain boundary (HAGBs, misorientation angle>15°) increases from 36.41% to 54.01%, this is why the increase of temperature promotes the growth of dynamically recrystallized grains. With the increase of hot deformation temperature, the recrystallized grains gradually increase and the number of corresponding deformed grains gradually decrease. However, by comparing the grain distribution diagram, the average grain size of the alloy increases with the increase of temperature, mainly because the recrystallized grains have shown a growth trend at higher temperature, it can be inferred that the increase of HAGBs means the decrease of storage dislocation density and the enhancement of dynamic recrystallization [40].

In order to study the texture evolution of composites under different thermal deformation conditions, the pole figures, inverse pole figures observed after thermal deformation of composites with crystal indexes {001}, {101}, {111} at 700 °C, 0.01s^{-1} and 900 °C, 0.01s^{-1} are studied, as shown in Fig. 7. As can be seen from Fig. 7 (a) and (c), under the deformation condition of 700 °C and 0.01s^{-1}, the maximum texture strength is 4.07. As the deformation temperature increases to 900 °C, the maximum texture strength is 3.78. As can be seen from Fig. 7 (b) and (d), under the deformation conditions of 700 °C and 0.01s^{-1}, the maximum texture strength is 2.70. As the deformation temperature increases to 900 °C, the texture strength decreases to 2.42. With the increase of temperature, the texture strength decreases, after the increase of temperature, the degree of recrystallization increases, more recrystallized grains appear, and the orientation distribution of recrystallized grains is more arbitrary, that is texture weakening occurs. With the increase of deformation temperature, fiber texture (silk texture) also changed to some extent. At lower temperature, it is mainly weak <001> and <101>//X, at 900 °C, it is mainly enhanced <101> and <111>//X.

In addition, the volume fraction of different component textures of the composite after thermal deformation is shown in Fig. 7 (e). At a lower deformation temperature of 700 °C, the {011} <100> goss texture, {011} <112> brass texture, {121} <111> copper texture, S texture, <111>//X, <110>//X and <100>//X are 6.58%, 6.54%, 9.2%, 7.99%, 21.8%, 46.9% and 19.0% respectively. At a higher deformation temperature of 900 °C, the volume fractions of texture components were 3.65%, 8.3%, 8.72%, 12.5%, 19.5%, 28.9% and 14.8%, respectively. It can be seen from the figure that the volume fraction of the main texture components of the composite that there are small changes in the composites (including goss texture, brass texture, copper texture and S texture) as the temperature increases to 900 °C, while the volume fraction of the corresponding randomly oriented grains decreases significantly.

The texture transformation is mainly due to the influence of dynamic recrystallization effect on the material during thermal deformation.

In fact, EBSD method can not only provide microstructure and crystal orientation information, but also study the distribution of plastic equivalent strain and Mises stress at grain scale, and even study the dislocation content. Using the nucleation average orientation difference method (KAM) to determine the local orientation difference of EBSD data, and simply calculate the geometric necessary dislocation (GND) density according to the strain gradient theory, we can quantitatively study the evolution of dislocation density under different state conditions [41–44]. Grain boundary migration plays an important role in dynamic recrystallization during thermal deformation. The migration of grain boundaries is related to dislocations near grain boundaries. Kam can quantitatively calculate the geometric dislocation density to reflect the homogenization degree of plastic deformation. Where the value is high, it means that the degree of plastic deformation is large or the defect density is high. Kam is a core point composed of 24 nearest adjacent points. It is used to assign a scalar value to each point to represent its local orientation difference. The Kam diagram obtained in EBSD can be used to calculate the geometric dislocation density, to judge the state of material stress distribution during deformation. Therefore, it is of great significance to study the dislocation density near the grain boundary of GO-Cu/CeO_2/Cr composites. The density of geometrically necessary dislocations (GND) is related to local dislocations, which can be expressed as [45,46]:

$$\rho^{GND} = 2\theta/\mu b \quad (11)$$

Where, ρ^{GND} represents the geometrically necessary dislocation density, m^{-2}, θ represents the average orientation, and the critical angle is set to 3°, exceeding this critical value will not be included in the calculation, μ is the step size of the scan, 0.1 μm, B is the Berger vector of copper, 2.55 nm.

The corresponding average angle values can be obtained from the Kam diagram in Fig. 8, and then the geometric necessary dislocation densities of GO-Cu/CeO_2/Cr composites at 700 °C, 0.01 s^{-1} and 900 °C and 0.01 s^{-1} are calculated respectively $\rho = 1.74 \times 10^{15}$ m^{-2} and $\rho = 1.52 \times 10^{15}$ m^{-2}, the dislocation density in the composite decreases with the increase of temperature, because the increase of temperature promotes the recrystallization process. At the same time, the dislocation is consumed to provide driving force for recrystallization in the recrystallization process, so that the dislocation density decreases continuously.

4. Conclusion

The thermal compression tests of Cu/CeO_2/Cr and GO-Cu/CeO_2/Cr composites at 0.001–1 s^{-1} strain rate and 600–900 °C deformation temperature was carried out by Gleeble-1500D simulator. The effect of graphene on Cu/CeO_2/Cr composites was discussed, and the following conclusions were drawn:

1. After isothermal thermal compression, Cr particles are extruded into strips. In the process of thermal compression, the strips elongate perpendicular to the compression direction.
2. The flow stress increases with the increase of strain rate or the decrease of deformation temperature. The small-size nanoparticles CeO_2 at the metal matrix interface to pin dislocations, inhibit dynamic recovery and dynamic recrystallization, and dispersion strengthening, grain refinement and twin formation all increase the flow stress of GO-Cu/CeO_2/Cr composites.
3. With the increase of deformation temperature, the degree of dynamic recrystallization gradually deepens, the volume fraction of main texture components such as goss texture, brass texture, copper texture and S texture changes little, and the volume fraction of the corresponding randomly oriented grains decreases significantly. The texture transformation is mainly due to the influence of dynamic recrystallization effect on the material during thermal deformation.
4. The constitutive equation of the composite is established. The activation energy of Cu/CeO_2/Cr composite is 164.174 kJ/mol. The addition of GO increased the activation energy of the composites by 27.99%–210.130 kJ/mol.

Declaration of competing interest

The authors declare that they have no known competing financial interests or personal relationships that could have appeared to influence the work reported in this paper.

Acknowledgments

This work was supported by the National Natural Science Foundation of China (52071134), Natural Science Foundation of Henan Province (202300410144), The Program for Innovative Research Team in University of Henan Province (22IRTSTHN001), China Postdoctoral Science Foundation (2021T140779) and Outstanding Talents Innovation Fund of Henan Province (ZYQR201912164), Scientific Research and Development Special Project of Henan Academy of Sciences (220910009).

REFERENCES

[1] Fouvry S, Jedrzejczyka P, Chalandonb P. Introduction of an exponential formulation to quantify the electrical endurance of micro-contacts enduring fretting wear: application to Sn, Ag and Au coatings. Wear 2011;271:1524–34. https://doi.org/10.1016/j.wear.2011.01.058.

[2] Shen F, Ke LL. Numerical study of coupled electrical-thermal-mechanical-wear behavior in electrical contacts.

Metals 2021;11(6):955–72. https://doi.org/10.3390/met11060955.
[3] Zhang XH, Zhang Y, Tian BH, Jia YL, Fu M, Liu Y, et al. Graphene oxide effects on the properties of Al_2O_3-Cu/35W5Cr composite. J Mater Sci Technol 2020;37(2):185–99. https://doi.org/10.1016/j.jmst.2019.08.014.
[4] Geng YF, Ban YJ, Wang BJ, Li X, Song KX, Zhang Y, et al. A review of microstructure and texture evolution with nanoscale precipitates for copper alloys. J Mater Sci Technol 2020;9(5):11918–34. https://doi.org/10.1016/j.jmrt.2020.08.055.
[5] Zhang XH, Zhang Y, Tian BH, Song KX, Liu P, Jia YL, et al. Review of nano-phase effects in high strength and conductivity copper alloys. Nanotechnol Rev 2019;8(1):383–95. https://doi.org/10.1515/ntrev-2019-0034.
[6] Song KX, Geng YF, Ban YJ, Zhang Y, Li Z, Mi XJ, et al. Effects of strain rates on dynamic deformation behavior of Cu-20Ag alloy. J Mater Sci Technol 2021;79(20):75–87. https://doi.org/10.1016/j.jmst.2020.11.043.
[7] Shukla AK, Narayana Murty SVS, Sharma SC, Mondal K. Constitutive modeling of hot deformation behavior of vacuum hot pressed Cu-8Cr-4Nb alloy. Mater Des 2015;75:57–64. https://doi.org/10.1016/j.matdes.2015.03.023.
[8] Zhang Y, Sun HL, Volinsky AA, Tian BH, Song KX, Wang BJ, et al. Hot workability and constitutive model of the Cu-Zr-Nd alloy. Vacuum 2017;146:35–43. https://doi.org/10.1016/j.vacuum.2017.09.017.
[9] Ban YJ, Zhang Y, Tian BH, Jia YL, Song KX, Li x, et al. Microstructure evolution in Cu-Ni-Co-Si-Cr alloy during hot compression by Ce addition. Materials 2020;13(14):3186–97. https://doi.org/10.3390/ma13143186.
[10] Yang PF, Zhou M, Zhang Y, Jia YL, Tian BH, Liu Y, et al. Effect of Y addition on microstructure evolution and precipitation of Cu-Co-Si alloy during hot deformation. Mater Char 2021;181:111502. https://doi.org/10.1016/J.MATCHAR.2021.111502.
[11] Hiraoka Y, Hanado H, Inoue T. Deformation behavior at room temperature of W-80vol%Cu composite. Int J Refract Metals Hard Mater 2004;22:87–93. https://doi.org/10.1016/j.ijrmhm.2004.01.002.
[12] Zhang XH, Zhang Y, Tian BH, An JC, Zhao Z, Volinsky AA, et al. Arc erosion behavior of the Al_2O_3-Cu/(W,Cr) electrical contacts. Composites Part B 2019;160:110–8. https://doi.org/10.1016/j.compositesb.2018.10.040.
[13] Zhang XH, Zhang Y, Tian BH, Jia YL, Liu Y, Song KX, et al. Thermal deformation behavior of the Al_2O_3-Cu/(W,Cr) electrical contacts. Vacuum 2019;164:361–6. https://doi.org/10.1016/j.vacuum.2019.03.054.
[14] Ban YJ, Zhang Y, Jia YL, Tian BH, Volinsky AA, Zhang XH, et al. Effects of Cr addition on the constitutive equation and precipitated phases of copper alloy during hot deformation. Mater Des 2020;191:108613. https://doi.org/10.1016/j.matdes.2020.108613.
[15] Liang SL, Liu S, Zhang Y, Zhou M, Tian BH, Geng YF, et al. Effect of in situ graphene-doped nano-CeO_2 on microstructure and electrical contact properties of Cu30Cr10W contacts. Nanotechnol Rev 2021;10(1):385–400. https://doi.org/10.1515/NTREV-2021-0031.
[16] Liu S, Li LH, Zhou M, Liang SL, Zhang Y, Huang JL, et al. Preparation and properties of graphene reinforced Cu/0.5$CeO_2$30Cr electrical contact materials. Vacuum 2022;195:110687. https://doi.org/10.1016/j.vacuum.2021.110687.
[17] Geng YF, Zhang Y, Song KX, Jia YL, Li X, Stock HR, et al. Effect of Ce addition on microstructure evolution and precipitation in Cu-Co-Si-Ti alloy during hot deformation. J Alloys Compd 2020;842:155666. https://doi.org/10.1016/j.jallcom.2020.155666.
[18] Ban YJ, Zhang Y, Tian BH, Song KX, Zhou M, Zhang XH, et al. EBSD analysis of hot deformation behavior of Cu-Ni-Co-Si-Cr alloy. Mater Char 2020;169:110656. https://doi.org/10.1016/j.matchar.2020.110656.
[19] Wang BJ, Zhang Y, Tian BH, An JC, Volinsky AA, Sun HL, et al. Effects of Ce addition on the Cu-Mg-Fe alloy hot deformation behavior. Vacuum 2018;155:594–603. https://doi.org/10.1016/j.vacuum.2018.06.006.
[20] Mirzadeh H, Parsa MH. Hot deformation and dynamic recrystallization of NiTi intermetallic compound. J Alloys Compd 2014;614:56–9. https://doi.org/10.1016/j.jallcom.2014.06.063.
[21] Ji GL, Li Q, Li L. A physical-based constitutive relation to predict flow stress for Cu-0.4Mg alloy during hot working. Mater Sci Eng 2014;615:247–54. https://doi.org/10.1016/j.msea.2014.07.082.
[22] Dong ZY, Jia SG, Zhao PF, Deng M, Song KX. Hot deformation behavior of Cu-0.6Cr-0.03Zr alloy during compression at elevated temperatures. Mater Sci Eng 2013;570:87–91. https://doi.org/10.1016/j.msea.2013.01.059.
[23] Ji GL, Yang G, Li L, Li Q. Modeling constitutive relationship of Cu-0.4 Mg alloy during hot deformation. J Mater Eng Perform 2014;23(5):1770–9. https://doi.org/10.1007/s11665-014-0912-0.
[24] Cheng WL, Bai Y, Ma SC, Wang LF, Wang HX, Yu H. Hot deformation behavior and workability characteristic of a fine-grained Mg-8Sn-2Zn-2Al alloy with processing map. J Mater Sci Technol 2019;35(6):1198–209. https://doi.org/10.1016/j.jmst.2018.12.001.
[25] Tahreen N, Zhang DF, Pan FS, Jiang XQ, Li DY, Chen DL, et al. Hot deformation and processing map of an as-extruded Mg-Zn-Mn-Y alloy containing I and W phases. Mater Des 2015;87:245–55. https://doi.org/10.1016/j.matdes.2015.08.023.
[26] Kabir ASH, Sanjari M, Su J, Jung IH, Yue S. Effect of strain-induced precipitation on dynamic recrystallization in Mg-Al-Sn alloys. Mater Sci Eng 2014;616:252–9. https://doi.org/10.1016/j.msea.2014.08.032.
[27] Sellars CM, Mctegart WJ. On the mechanism of hot deformation. Acta Metall 1966;14(9):1136–8. https://doi.org/10.1016/0001-6160(66)90207-0.
[28] Zener C, Hollomon JH. Effect of Strain Rate Upon Plastic Flow of Steel 1944;15(1):22–32. https://doi.org/10.1063/1.1707363.
[29] Zhou MY, Liu XH, Yue HF, Liu SC, Ren LB, Xin Y, et al. Hot deformation behavior and processing maps of hybrid SiC and CNTs reinforced AZ61 alloy composite. J Alloys Compd 2021;868:159098. https://doi.org/10.1016/j.jallcom.2021.159098.
[30] Wu YT, Li C, Xia XC, Liang HY, Qi QQ, Liu YC. Precipitate coarsening and its effects on the hot deformation behavior of the recently developed γ'-strengthened superalloys. J Mater Sci Technol 2021;67:95–104. https://doi.org/10.1016/j.jmst.2020.06.025.
[31] Liang SL, Zhou M, Zhang Y, Liu S, Li X, Tian BH, et al. Thermal deformation behavior of GO/CeO_2 in-situ reinforced Cu30Cr10W electrical contact material. J Alloys Compd 2021;899:16266. https://doi.org/10.1016/j.jallcom.2021.163266.
[32] Zhao Z, Zhang Y, Tian BH, Jia YL, Liu Y, Song KX, et al. Co effects on Cu-Ni-Si alloys microstructure and physical properties. J Alloys Compd 2019;797:1327–37. https://doi.org/10.1016/j.jallcom.2019.05.135.
[33] Fu Y, Xiao WL, Kent D, Dargusch MS, Wang JS, Zhao XQ, et al. Ultrahigh strain hardening in a transformation-induced plasticity and twinning-induced plasticity titanium alloy. Scripta Mater 2020;187:285–90. https://doi.org/10.1016/j.scriptamat.2020.06.029.
[34] Mishnev R, Shakhova I, Belyakov A, Kaiby-shev R. Deformation microstructures, strengthening mechanisms,

and electrical conductivity in a Cu-Cr-Zr alloy. Mater Sci Eng 2015;629:29–40. https://doi.org/10.1016/j.msea.2015.01.065.
[35] Bittner F, Yin S, Kauffmann A, Freudenberger J, Klauß H, Korpala G, et al. Dynamic recrystallisation and precipitation behaviour of high strength and highly conducting Cu-Ag-Zr-alloys. Mater Sci Eng 2014;597:139–47. https://doi.org/10.1016/j.msea.2013.12.051.
[36] Geng YF, Li X, Zhou HL, Zhang Y, Jia YL, Tian BH, et al. Effect of Ti addition on microstructure evolution and precipitation in Cu-Co-Si alloy during hot deformation. J Alloys Compd 2020;821:153518. https://doi.org/10.1016/j.jallcom.2019.153518.
[37] Lei Q, Li Z, Hu WP, Liu Y, Meng XL, Derby B, et al. Microstructure evolution and hardness of an ultra-high strength Cu-Ni-Si alloy during thermo-mechanical processing. J Mater Eng Perform 2016;25(7):2615–25. https://doi.org/10.1007/s11665-016-2147-8.
[38] Sidor JJ, Kestens LAI. Analytical description of rolling textures in face-centred-cubic metals. Scripta Mater 2013;68(5):273–6. https://doi.org/10.1016/j.scriptamat.2012.10.039.
[39] He WJ, Chapuis A, Chen X, Liu Q. Effect of loading direction on the deformation and annealing behavior of a zirconium alloy. Mater Sci Eng 2018;734:364–73. https://doi.org/10.1016/j.msea.2018.08.013.
[40] Geng YF, Li X, Zhang Y, Jia YL, Zhou HL, Tian BH, et al. Microstructure evolution of Cu-1.0Co-0.65Si-0.1Ti alloy during hot deformation. Vacuum 2020;177:109376. https://doi.org/10.1016/j.vacuum.2020.109376.
[41] Calcagnotto M, Ponge D, Demir E, Raabe D. Orientation gradients and geometrically necessary dislocations in ultrafine grained dual-phase steels studied by 2D and 3D EBSD. Mater Sci Eng 2010;527(10):2738–46. https://doi.org/10.1016/j.msea.2010.01.004.
[42] Gao H, Huang Y, Nix WD, Hutchinson JW. Mechanism-based strain gradient plasticity-I. Theory. J Mech Phys Solid 1999;47:1239–63. https://doi.org/10.1016/s0022-5096(98)00103-3.
[43] Kubin LP, Mortensen A. Geometrically necessary dislocations and strain-gradient plasticity: a few critical issues. Scripta Mater 2003;48(2):119–25. https://doi.org/10.1016/S1359-6462(02)00335-4.
[44] Ma XL, Huang CX, Moering J, Ruppert M, Hoppel HW, Goken M, et al. Mechanical properties of copper/bronze laminates: role of interfaces. Acta Mater 2016;116:43–52. https://doi.org/10.1016/j.actamat.2016.06.02.
[45] Wu YS, Qin XZ, Wang CS, Zhou LZ. Influence of phosphorus on hot deformation microstructure of a Ni-Fe-Cr based alloy. Mater Sci Eng 2019;768:138454. https://doi.org/10.1016/j.msea.2019.138454.
[46] Wu YS, Liu Z, Qin XZ, Wang XS, Zhou LZ. Effect of initial state on hot deformation and dynamic recrystallization of Ni-Fe based alloy GH984G for steam boiler applications. J Alloys Compd 2019;795:370–84. https://doi.org/10.1016/j.jallcom.2019.05.022.